J Solid State Electrochem (2003) 7: 607–613
DOI 10.1007/s10008-003-0390-z

ORIGINAL PAPER

E. I. Santiago · M. J. Giz · E. A. Ticianelli

Studies of carbon monoxide oxidation on carbon-supported platinum-osmium electrocatalysts

Received: 7 October 2002 / Accepted: 14 April 2003 / Published online: 1 July 2003

Abstract The electrocatalytic oxidation of hydrogen in the presence of carbon monoxide was studied on PtOs/C electrocatalysts prepared by the formic acid method and heat-treated under several temperatures and atmospheres. The physical properties of the metallic phase were evaluated by X-ray diffraction (XRD), energy dispersive X-ray (EDX) analysis, and in situ X-ray absorption spectroscopy (XAS). The electrochemical performance of these materials was evaluated by single-cell polarization measurements, cyclic voltammetry, and linear sweep CO stripping voltammetry. The results have shown an enhancement of the CO oxidation process for the as-prepared PtOs/C and for a material heat-treated in a reducing atmosphere (hydrogen at 500 °C), compared to Pt/C. The electrochemical data also showed that the as-prepared and hydrogen-treated PtOs/C catalysts present CO tolerance higher than Pt/C. This has been associated with the occurrence of a surface reaction of CO adsorbed on Pt and oxygenated Os sites, favored by an intimate physical contact between segregated Os and Pt phases.

Keywords Carbon monoxide · Extended X-ray absorption fine structure · Platinum-osmium · X-ray absorption spectroscopy · X-ray near-edge structure

Introduction

Carbon-supported platinum catalysts are usually employed at the anode of proton exchange membrane fuel cells (PEMFC), but this material is only satisfactory to promote the hydrogen oxidation reaction (HOR) with high efficiency when pure H_2 is used. In the case of the gas obtained by reforming other fuels such as methanol, ethanol, or formic acid, the carbon monoxide produced as a poisoning by-product causes a drastic decrease of the anode performance and thus of the fuel cell energy density [1, 2].

For a poisoned anode, the current is generated by the oxidation of hydrogen only on platinum sites free of adsorbed CO. In order to enhance the CO tolerance of the fuel cell anode, several binary electrocatalysts composed of Pt and an oxophilic element, such as Pt-Ru or Pt-Sn, have been developed [3, 4, 5, 6, 7, 8]. In most cases, a bifunctional mechanism [7] has been proposed to explain the poisoning/tolerance effect. According to this model, the poisoning effect is reduced owing to the occurrence of a surface reaction between the CO adsorbed on the platinum sites and oxygenated species produced at neighboring oxophilic sites.

However, there are still many controversies about the nature of the CO tolerance mechanisms. McBreen and Mukerjee [9] have suggested that an electronic effect induced by the insertion of Ru into the Pt structure in a PtRu alloys results in an increase of the CO tolerance due to a weakening of the Pt–CO interaction. More recently, Watanabe et al. [10, 11] reported that the bifunctional theory could not be accepted for Pt-non-precious metal alloys, such as PtFe, PtCo, and PtNi, and this was related to the formation of a Pt skin layer on the alloy particles. However, it has been found that for Pt alloys with precious metals, such as Ru, Os, or Re, the bifunctional mechanism is operative due to the stability of these elements in the Pt structure. Also, Rolison and co-workers [12] have demonstrated that an improvement of the CO tolerance can be achieved at RuO_xHy and Pt intimate phase neighbors, demonstrating that for the bifunctional mechanism the surface conditions are more important than the presence of a true alloy itself.

In order to analyze the interactions between Pt and the second element, binary electrocatalysts have been characterized by X-ray absorption spectroscopy (XAS)

Dedicated to Prof. Wolf Vielstich on the occasion of his 80th birthday in recognition of his numerous contributions to interfacial electrochemistry

E. I. Santiago · M. J. Giz · E. A. Ticianelli (✉)
Instituto de Química de São Carlos, Universidade de São Paulo, C.P. 780, CEP 13560-970 São Carlos, SP, Brazil
E-mail: edsont@iqsc.usp.br

under electrochemical conditions [13, 14, 15]. Because of its atomic selectivity, this technique allows the study of the effect of the second element in the alloys on the Pt–Pt bond distance, the coordination number, and the occupancy of the 5d band of the platinum atoms. It has been found that the extent of the modifications on these parameters depends on the nature of the metal bonded to platinum and leads to different kinetic behavior of the hydrogen oxidation reaction and the CO poisoning characteristics, eventually resulting in changes in activation energies, reaction orders, or CO surface coverage.

Among several binary alloys, a Pt-Ru electrocatalyst has been presented as a promising CO-tolerant material. However, for CO concentrations of 100 ppm at 85 °C, a high overpotential is still observed for hydrogen oxidation, with losses of about 270 mV at 1 A cm^{-2} [16]. In this context, other electrocatalysts based on platinum and other oxophilic elements have been widely studied in the search for CO-tolerant systems and for understanding the involved processes. The electrocatalytic activity of binary alloys is also strongly dependent on the methodology of the material preparation, since the surface reaction involving CO depends on the particle size and the distribution of the atoms on its surface [17, 18].

Because of the similarities between Os and Ru, Os-based electrocatalysts could provide satisfactory CO tolerance. In this context, the electrocatalytic mechanism for CO, methanol, and ethanol oxidation on smooth electrodes with codeposited, electrodeposited, and spontaneously deposited Os-based catalysts has been reported [19, 20, 21, 22]. In all cases, an enhancement of the electrocatalytic activity has been observed for Os-deposited electrocatalysts, but the best results are those for Os incorporated into ternary or quaternary materials [23, 24]. Some limitations on the performance of these materials have been attributed to the formation of inactive Os species, such as OsO_2.

The aim of this work is to characterize and evaluate the electrocatalytic activity for the hydrogen and CO oxidation reactions of carbon-supported PtOs/C electrocatalysts. Studies were conducted using in-situ XAS and standard electrochemical techniques, such as single-cell polarization measurements, cyclic voltammetry, and linear sweep CO stripping voltammetry. The effects of heat treatment under air (200 °C) and under hydrogen (500 °C) on the PtOs/C catalyst in the electrocatalytic activity are also characterized.

Experimental

The electrocatalysts based on PtOs/C were obtained by the reduction of dihydrogen hexachloroplatinate (H_2PtCl6; Aldrich, 37%) and dihydrogen hexachloroosmate (H_2OsCl6; Aldrich) with formic acid, in the presence of carbon powder (Vulcan XC-72, Cabot) [25], using 20 wt% as the metal/carbon ratio. After reduction of the metal ions, the materials were filtered and dried at 80 °C for 2 h. The same procedure was applied to prepare Pt/C (20 wt%) electrocatalysts used for comparison. The materials were submitted to heat treatments at oxidizing (air) and reducing (hydrogen) atmospheres at 200 °C and 500 °C, respectively. The atomic composition of the Pt-Os catalyst was determined by energy dispersive X-ray analysis (EDX; Zeiss model DSM 960). The particle mean size was determined by X-ray diffraction with Cu K_∞ radiation in the 2θ range from 30° up to 90°.

Gas diffusion electrodes for PEMFC were prepared as described in the literature [26]. The metal loading was always 0.35 mg cm^{-2}, achieved using Pt/C E-Tek for the cathodes and PtOs/C for the anodes, in both cases with 1.1 mg Nafion cm^{-2} in the catalyst layer. The gas diffusion layer consisted of carbon powder (Vulcan XC-72, Cabot) with 15 wt% of polytetrafluoroethylene (PTFE; TE-306A, Du Pont), deposited onto a carbon cloth substrate (PWB-3, Stackpole). Nafion 115 membranes (H^+, Du Pont) were used as the electrolyte. The membrane and electrode assemblies (MEA) were prepared by hot pressing the anode and the cathode to a membrane at 125 °C and 1000 kg cm^{-2} for 2 min, as described previously [26].

Polarization curves were obtained galvanostatically with the single cell at 85 °C, using oxygen saturated with Milli-Q water at 90 °C and 1.7 atm, and either pure hydrogen or a mixture of hydrogen with CO (100 ppm) saturated with water at 100 °C and 2.0 atm. Before data acquisition the system was kept at 0.7 V with pure hydrogen for 2 h and at 0.8 V with the H_2/CO mixture for another 2 h in order to reach the steady-state poisoning condition.

Linear sweep CO stripping and cyclic voltammograms of the anodes were obtained on the gas diffusion electrodes with a potentiostat-galvanostat (Solartron model 1285). In these experiments the PtOs/C anode was used as the working electrode, while the Pt/C to which a continuous injection of H_2 was applied was used as the counter and the hydrogen reference electrodes (HRE). The linear sweep CO stripping measurements were carried out after the injection of pure CO in the anode at 0.2 V vs. HRE for 10 min, followed by argon for 30 min, to remove the excess of CO. The stripping and cyclic voltammograms were recorded at 10 mV s^{-1} at room temperature.

The ''in situ'' X-ray absorption spectroscopy (XAS) measurements were performed using a homemade spectroelectrochemical cell [27]. The working electrodes consisted of pellets formed with 6 mg cm^{-2} of dispersed catalysts, mixed with 30 wt% Nafion perfluorinated ion-exchange powder (Aldrich, 5 wt%) and agglutinated with PTFE (ca. 40 wt%). Measurements were made at several electrode potentials (referred to the reversible hydrogen electrode, RHE) in 0.5 M H_2SO_4 solutions. The preparation of the counter electrodes followed the same procedure, but using a Pt/C catalyst. These electrodes were cut in the center, in order to allow free passage of the X-ray beam. Prior to the experiments the electrodes were soaked in the electrolyte for at least 48 h. The measurements were carried out at the Pt L_3 edge (11,564 eV), with energy scans from 11,440 up to 12,200 eV, which include the XANES (X-ray near-edge structure) and EXAFS (extended X-ray absorption fine structure) regions. The materials were also evaluated at the Os L_3 edge (10,870 eV), but only in the in XANES region (10,840 up to 10,910 eV).

All experiments were conducted at the XAS beam line in the National Synchrotron Light Source Laboratory (LNLS), Brazil. The data acquisition system for XAS comprised three ionization detectors (incidence I_o, transmitted I_t, and reference I_r). The reference channel was employed primarily for internal calibration of the edge positions by using a pure Pt foil. Air was used in the I_o, I_t, and I_r chambers. Owing to the low critical energy of the LNLS storage ring (2.08 keV), third-order harmonic contamination of the Si(111) monochromatic beam is expected to be negligible above 5 keV [28].

The computer program used for data analysis was the WinXAS package [29]. This was done according to procedures described in detail in the literature [30, 31]. Briefly, the XANES spectra were first corrected for background absorption by fitting the pre-edge data (from −60 to −20 eV below the edge) to a linear formula, followed by extrapolation and subtraction from the data over the energy range of interest. Next, the spectra were calibrated for the edge position using the second-derivative method and the data

from the reference channel. Finally, the spectra were normalized, taking as reference an average line generated throughout the EXAFS region. The EXAFS oscillations were removed from the measured absorption coefficient using a cubic spline background subtraction. Next, the EXAFS were converted to signal per absorbing atom by dividing by the height of the absorbing edge given by the fitted spline function. Fourier transforms (k^3 weighted) of the EXAFS oscillations were obtained employing the Bessel window.

Results and discussion

Physical characterization

The EDX analysis showed that the total Pt:Os atomic composition for PtOs/C is 90:10. The X-ray diffractograms for PtOs/C treated at different temperatures are shown in Fig. 1. Only the presence of crystalline planes for Pt (111), (200), (222), and (311) were identified, with no additional osmium phases (Os or OsO_2) [32]. For the air-treated material, the absence of diffraction peaks for Os oxides can be related to the presence of a too low Os content, which also may be in the form of an amorphous oxide phase. After the heat treatment under hydrogen, just a better definition of the Pt peaks is observed and this is related to an increase of the particle size. There are no changes in the peak positions compared to the other materials, indicating the absence of interactions between the Pt and Os atoms, probably because they are accommodated in separate phases.

The average metallic particle size for the materials treated at different temperatures was determined by the Scherrer equation [33] using the (220) XRD peak, because it is less affected by the presence of other phases which may be present at a low content. The values of particle sizes are presented in Table 1. An increase of the particle size with the increase of the heat-treatment temperature is clearly seen, indicating the occurrence of an agglomeration of the smaller particles and, as a consequence, a decrease of the catalyst active surface area.

Figure 2 shows the Pt L_3 XANES spectra at 0.1 V vs. RHE obtained for the as-prepared, the air-treated (200 °C), and the H_2-treated (500 °C) PtOs/C catalysts. Figure 3 shows the results for the material treated at 500 °C in a H_2 atmosphere at several electrode potentials. In both cases the results for a Pt foil are presented for comparison. The absorption at the Pt L_3 edge (11,564 eV) corresponds to $2p_{3/2}$–5d electronic transitions and the magnitude of the hump (white line) located at about 5 eV is directly related to the occupancy of the 5d electronic states [34, 35].

The results in Fig. 2 are in agreement with those obtained from "in situ" XANES measurements for some Pt/C catalysts at 0.5 V in H_2SO_4 solutions [36]. It is seen that the results for the as-prepared material and the PtOs/C heat-treated at 500 °C in H_2 are similar to that for the Pt foil (Fig. 2). This indicates the absence of any interaction between Pt and Os atoms, which is consistent with the presence of segregated Pt and Os phases in the catalysts, as also suggested by the XDR results. However, for the material heat-treated at 200 °C

Table 1 Average particle size for PtOs/C prepared at different temperatures and atmospheres for the heat treatment

Catalyst	Average particle size (nm)
PtOs/C, as-prepared	2.8
PtOs/C, 200 °C, air	4.1
PtOs/C, 500 °C, H_2	7.4

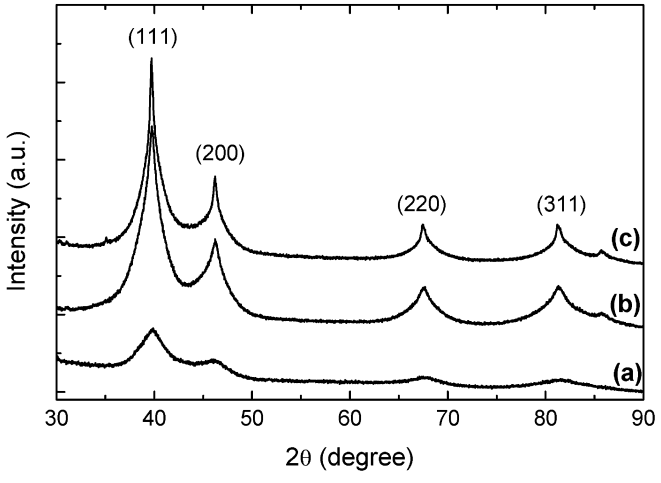

Fig. 1 X-ray diffraction patterns for PtOs/C: (*a*) as-prepared; (*b*) 200 °C, air; (*c*) 500 °C, H_2

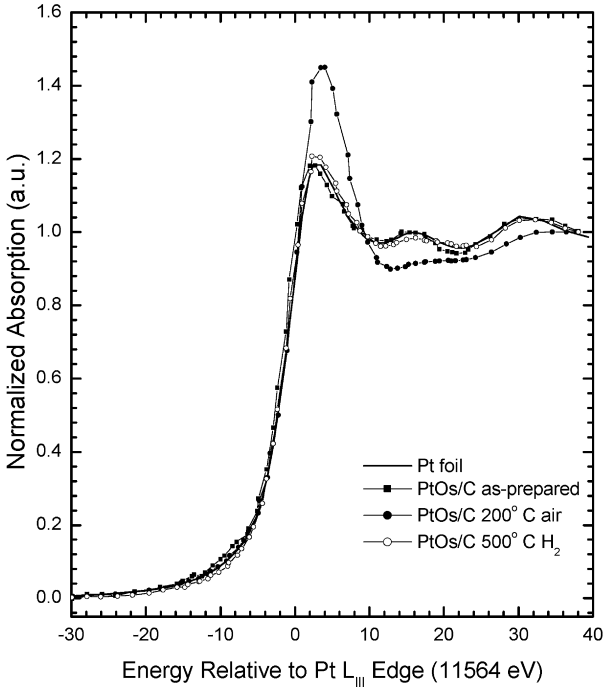

Fig. 2 XANES spectra at the Pt L_3 edge at 0.1 V vs. RHE for PtOs/C heat-treated at different atmospheres and temperatures

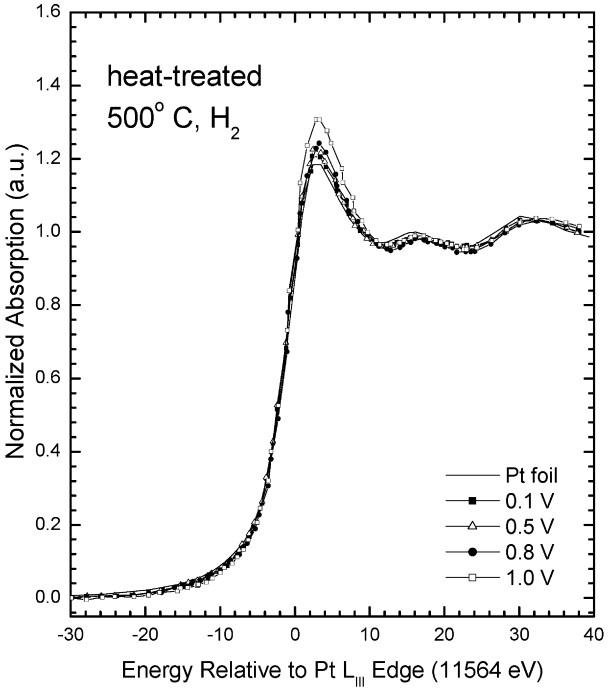

Fig. 3 XANES spectra at the Pt L_3 edge at several electrode potentials for PtOs/C heat-treated at 500 °C under hydrogen

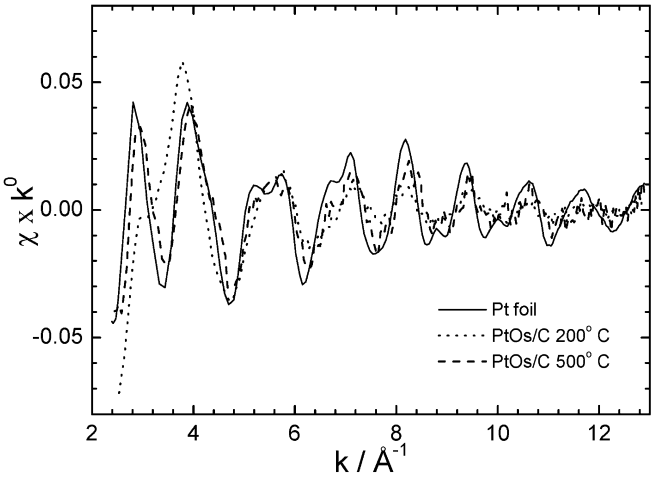

Fig. 4 EXAFS signal at the Pt L_3 edge at 0.1 V vs. RHE for PtOs/C heat-treated at different atmospheres and temperatures

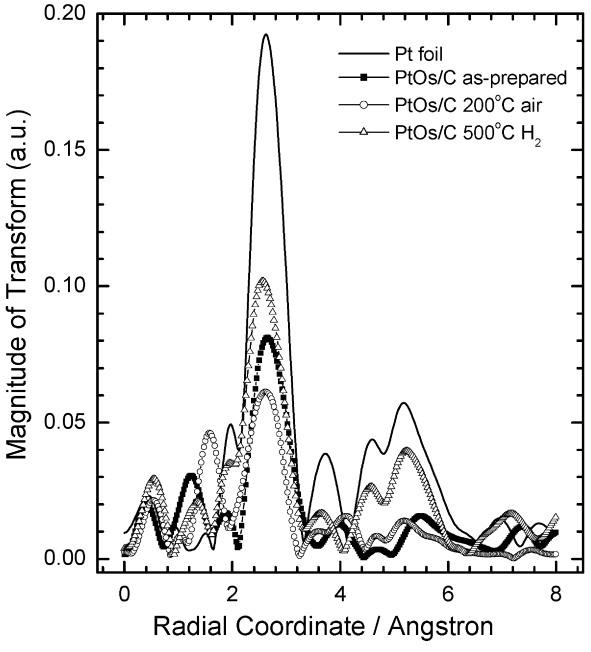

Fig. 5 Fourier transform (k^3 weighted) of the EXAFS oscillations at the Pt L_3 edge for PtOs/C heat-treated at different atmospheres and temperatures; $\Delta r = 3.6$–12.6 Å^{-1}

in air, an increase of the white line is seen, indicating lower occupancy of the Pt 5d electronic states, in agreement with the presence of an electron-withdrawing effect of the oxygen present on a Pt oxide phase. It is also seen that the white line magnitude does not appreciably change with the increase in the particle size (from 2.8 nm up to 7.1 nm).

The results in Fig. 3 show that above 0.8 V there is an increase of the white line magnitude in the XANES for Pt in the PtOs/C catalyst heat-treated at 500 °C under H_2. The same effect of the electrode potential was observed for all other PtOs/C catalysts (results not shown). In all cases the phenomenon can be attributed to the emptying of the Pt 5d band due to the well-known formation of a surface oxy-hydroxide layer on the catalyst particles at potentials above 0.85 V [34, 35, 36].

Figure 4 presents normalized EXAFS data for the Pt foil and for some of the PtOs/C electrocatalysts. The EXAFS function contains the superimposition of contributions of several coordination shells, and thus the Fourier transform technique is used to separate the signals. In this case, the peaks in the radial structure correspond to the contribution of individual coordination shells around the metallic atom under investigation [31]. These results are presented in Fig. 5 for all catalysts investigated in this work.

The similarity of the FT features in Fig. 5 indicates that the Pt phase present in all the catalysts is the fcc structure of bulk platinum. The peak centered at ~2.5 Å represents the contribution of the first metal–metal coordination shell to the EXAFS oscillations. It is seen that the magnitude of this peak is smaller for the dispersed catalysts, compared to that of bulk Pt, and this is just due to the very small particle size, as observed in a previous Pt/C study [35]. In contrast to real alloys, for example PtRu/C [35, 36], a single peak is apparent for all materials and this is evidence for the absence of direct coordination of Pt with Os atoms, meaning that they are located in segregated phases, as also evidenced by the XRD and XANES results. For the PtOs/C treated at 200 °C in air, the presence of a strong peak at around 1.5 Å is related to the presence of Pt–O coordination in a metal oxide phase, as also seen from the XANES results.

The XANES results obtained at the Os L_3 edge are presented in Fig. 6a and Fig. 6b for the as-prepared and for PtOs/C treated at 500 °C in H_2, respectively, for several electrode potentials. As for Pt, adsorptions at the Os L_3 edge are due to $2p_{3/2}$–5d electronic transitions. An enhancement of the white lines, compared to that of the Os foil, is observed even when both catalysts are polarized at 0.1 V, and this is indicative of the presence of an Os oxide phase in the sample. As in the case of Pt, there is an increase of the edge hump with the increase of the electrode potential, but this starts at much lower potentials because of the high oxophilic character of Os.

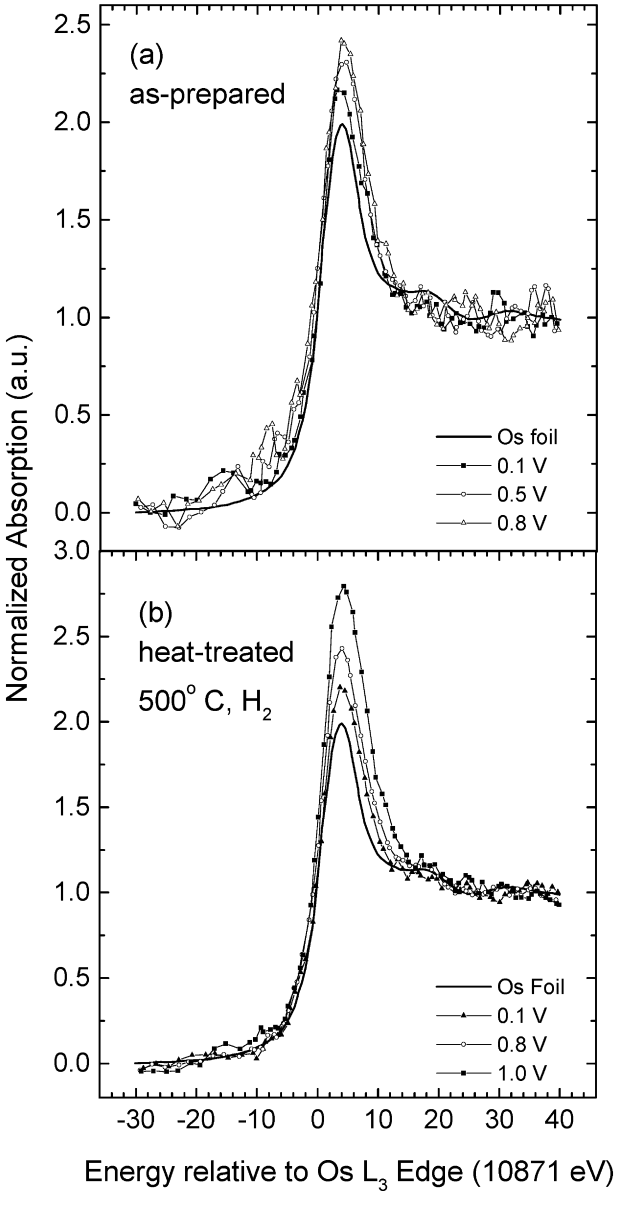

Fig. 6 XANES spectra at the Os L_3 edge at several electrode potentials: (**a**) as-prepared PtOs/C; (**b**) PtOs/C heat-treated at 500 °C under H_2

Electrochemical characterization

Figure 7 presents the cyclic voltammograms for the Pt/C and PtOs/C catalysts. The presence of the hydrogen absorption and desorption processes characteristic of Pt electrodes in acidic media is clearly evidenced for all catalysts. The PtOs/C electrodes present some changes in the hydrogen processes due to the distinct effects of the heat treatment; however, a pair of peaks associated with reversible conversion of Os to OsO_2, located at 0.65 V vs. RHE, is not observed [22].

The as-prepared material shows an enhancement of the (110) Pt–H oxidation charge (the oxidation peak at around 0.1 V), in agreement with the presence of a large atomic surface fraction of Pt atoms in that facet, as typically observed for very small catalyst particles [37]. As seen above, for the material treated in the oxidizing atmosphere (200 °C/air), the formation of Pt and Os surface oxide layers is clearly observed. After treatment in a reductive atmosphere at a higher temperature (500 °C, H_2), an increase of particle size and the reduction of Pt oxides take place. However, in Fig. 7 it is seen that the cyclic voltammograms present similar features for both materials. Thus, after the hydrogen treatment, the increase of catalyst activity due to the oxide reduction must be compensated by the loss of surface area caused by the increase of particle size.

The linear sweep CO stripping voltammograms obtained at 25 °C are shown in Fig. 8. The CO oxidation processes start at around 0.7 V on Pt/C, while for as-prepared PtOs/C the onset of CO oxidation occurs close to 0.6 V. After treatment under air, the CO oxidation is largely retarded and this is due to a blocking effect arising from the formation of inactive Pt and Os surface layers. The material treated under hydrogen shows intermediary catalytic activity for CO oxidation, compared to the other materials. This complex behavior is the result of the several effects of this heat treatment, as

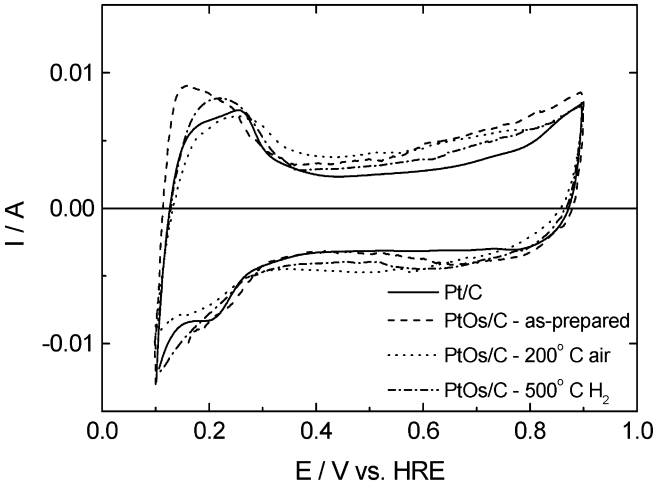

Fig. 7 Cyclic voltammograms for the PtOs/C electrodes; $T = 25$ °C; $v = 10$ mV s^{-1}

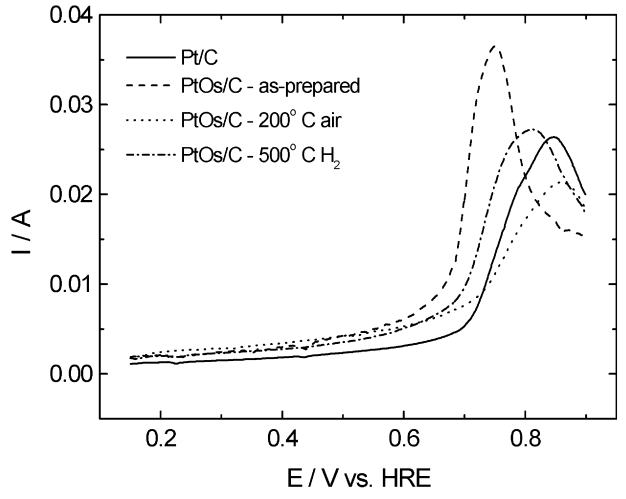

Fig. 8 Linear sweep CO stripping voltammograms for the PtOs/C electrodes; $T = 25$ °C; $v = 10$ mV s^{-1}

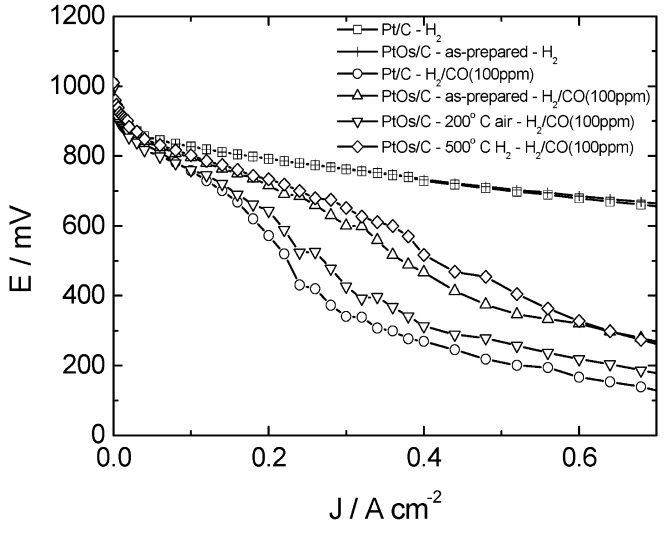

Fig. 9 Polarization curves for a single fuel cell using PtOs/C as the anode, fed with O_2 in the cathode, and H_2/CO (100 ppm) in the anode; $T_{cell} = 85$ °C, oxygen humidifier at 90 °C, and hydrogen humidifier at 100 °C; $P_{H2} = 2.0$ atm; $P_{O2} = 1.7$ atm

pointed out above in the analysis of the cyclic voltammogram features.

Figure 9 shows steady-state polarization curves for different PtOs/C electrocatalysts for the fuel cell anode supplied with pure hydrogen and hydrogen poisoned with CO (H_2/100 ppm CO). Results for a Pt/C anode are also shown for comparison. A very low electrocatalytic activity is observed for Pt/C and the oxidized air-treated PtOs/C catalysts when a CO-containing gas is introduced in the anode. The existence of oxidized Pt and Os species in the second material is clearly evidenced by the XANES experiments and these are mostly electrochemically inactive, as seen from the cyclic voltammetric experiments. The presence of this oxide layer may also promote a loss of active area for the hydrogen oxidation reaction and, consequently, a lowering of the electrocatalytic performance of the anode in the single cell.

For the as-prepared and the reduced PtOs/C catalysts, an enhanced performance is observed. This improved CO tolerance can be primarily explained by the presence of Os, which is able to produce active oxygenated species at very low potentials (see Fig. 6), as required by the bifunctional mechanism. This mechanism must be operating even though the results of XRD and XAS show the presence of segregated Os and Pt phases. Thus one may conclude that these phases are in very intimate physical contact. The effect of the increase of the particle size occurring after H_2 heat-treatment is not determinant for the polarization behavior, meaning that the effect of the reduction of the surface area must be compensated by a counteracting effect coming from the reduction of the inactive Pt and Os surface oxide phases.

Conclusions

XRD and XAS experiments conducted on PtOs/C electrocatalysts have demonstrated the formation of segregated Pt and Os phases and no interaction between the Pt and Os atoms. On the other hand, PtOs/C presents higher CO tolerance than Pt/C, and this is associated with the occurrence of the bifunctional mechanism favored by an intimate physical contact between the Os and Pt phases. The effect of the increase of particle size caused by the heat treatment under hydrogen is not determinant for the CO tolerance, meaning that the lowering of the surface area must be compensated by a counteracting effect coming from the reduction of inactive Pt and Os surface oxide phases.

Acknowledgements The authors thank the Fundação de Amparo a Pesquisa do Estado de São Paulo (FAPESP, procs. 00/12690-1 and 99/06430-8) for financial support and the Syncrotron Light Source Laboratory (LNLS, Brazil).

References

1. Markovic NM, Gasteiger HA, Ross PN, Jiang X, Villegas I, Weaver MJ (1995) Electrochim Acta 40:91
2. Biswas PC, Nodasaka Y, Enyo M (1996) J Appl Electrochem 26:30
3. Iannielo R, Schmidt VM, Stimming U, Stumper J, Wallau A (1994) Electrochim Acta 39:1863
4. Gasteiger HA, Markovic N, Ross PN, Cairns EJ (1994) J Phys Chem 98:617
5. Wang SR, Fedkiw PS (1992) J Electrochem Soc139:3151
6. Lee SJ, Mukerjee S, Ticianelli EA, McBreen J (1999) Electrochim Acta 44:3283
7. Watanabe M, Motoo S (1975) Electroanal Chem Interfacial Electrochem 60:267
8. Beden B, Lamy C, Tacconi NR, Arvia C (1990) Electrochim Acta 35:691
9. McBreen J, Mukerjee S (1995) J Electrochem Soc 142:3399

10. Watanabe M, Zhu Y, Igarashi H, Uchida H (2000) Electrochemistry 68:244
11. Watanabe M (2003) In: Vielstich W, Gasteiger H, Lamm A (eds) Handbook of fuel cells: fundamentals, technology and applications, vol 2. Wiley, Chichester, UK, pp 408–415
12. Long JW, Stroud RM, Swider-Lyons KE, Rolison DR (2000) J Phys Chem B 104:9772
13. Mukerjee S, McBreen J (1997) In: Savadogo O (ed) New materials for fuel cells and modern battery systems II (Proceedings of the 2nd international symposium on new materials for fuel cells and modern battery systems, Montreal, Canada, 6–10 July 1997), pp 548–559
14. Mukerjee S (1990) J Appl Electrochem 20:537
15. Vogel W, Lundquist J, Ross P, Stonehart P (1975) Electrochim Acta 20:79
16. Oetjen HF, Schmidt VM, Stimming U, Trila F (1996) J Electrochem Soc 143:3838
17. Iwasita T, Hoster H, John-Anacker A, Lin WF, Vielstich W (2000) Langmuir 16:522
18. Hoster H, Iwasita T, Baumgärtner H, Vielstich W (2001) Phys Chem Chem Phys 3:337
19. Petrii AO, Kalinin VD (1999) Russ J Electrochem 35:627
20. Crown A, Moraes IR, Wieckowski A (2001) J Electroanal Chem 500:333
21. Zhu Y, Cabrera CR (2001) Electrochem Solid-State Lett 4:A45
22. Orozco G, Gutiérrez C (2000) J Electroanal Chem 484:64
23. Ley KL, Liu R, Pu C, Fan Q, Leyarovska N, Segre C, Smotkin ES (1997) J Electrochem Soc 144:1543
24. Gurau B, Viswanathan R, Liu R, Lanfrez TJ, Ley K, Smotkin ES, Reddington E, Sapienza A, Chan C, Mallouk TE, Sarangapani S (1998) J Phys Chem B 102:9997
25. Pinheiro ALN, Oliveira-Neto A, de Souza EC, Perez J, Paganin VA, Ticianelli EA, Gonzalez ER (2003) J New Mater Electrochem Syst 6:1
26. Paganin VA, Ticianelli EA, Gonzalez ER (1996) J Appl Electrochem 26:297
27. McBreen J, O'Grady WE, Pandya KI, Hoffman RW, Sayers DE (1987) Langmuir 3:428
28. Tolentino H, Cezar JC, Cruz DZ, Compagnon-Caillol V, Tamura E, Alves MC (1998) J Synchrotron Radiat 5:521
29. Ressler (1997) J Phys IV C2:269
30. Pandya KI, Hoffman RW, McBreen J, O'Grady WE (1990) J Electrochem Soc 137:383
31. van Zon JBAC, Koningsberger DC, Van't Blik HFJ, Sayers DE (1985) J Chem Phys 82:5742
32. McClune WF (1983) Powder diffraction file: inorganic phases. International Centre for Diffraction Data, Swarthmore, file numbers 4-802, 6-662, 22-120
33. Cullity BD (1967) Elements of X-ray diffraction. Addison-Wesley, Boston, p 99
34. Min MK, Cho J, Cho K, Kim H (2000) Electrochim Acta 45:4211
35. McBreen J, Mukerjee S (1995) J Electrochem Soc 142:3399
36. Camara GA, Giz MJ, Paganin VA, Ticianelli EA (2002) J Electroanal Chem 537:21
37. Kinoshita K (1990) J Electrochem Soc 137:845